

# Analysis and control of genetic toggle switches subject to periodic multi-input stimulation

Davide Fiore<sup>1</sup>, Agostino Guarino<sup>1</sup>, Mario di Bernardo<sup>1,2</sup>

**Abstract**—In this paper, we analyze a genetic toggle switch recently studied in the literature where the expression of the two repressor proteins can be tuned by controlling two different inputs, namely the concentration of two inducer molecules in the growth medium of the cells. Specifically, we investigate the dynamics of this system when subject to different periodic stimuli and we provide an analytical model that captures qualitatively the experimental observations and approximate its asymptotic behaviour. We also discuss the effect that the system parameters have on the prediction accuracy of the model. Moreover, we propose a possible external control strategy to regulate the mean value of the fluorescence of the reporter proteins when the cells are subject to such periodic forcing.

## I. INTRODUCTION

The genetic toggle switch is a fundamental component in synthetic biology as it plays a major role in cell differentiation and decision making [1], [2]. Its importance comes from its ability to endow host cells with memory of some previous stimulus reporting this information as high expression rate of a specific repressor protein [3]–[5].

The genetic toggle switch as first designed by [3] consists of two repressor proteins, both repressing each other's promoter, so that only one protein is fully expressed at any time. From a modelling viewpoint, the genetic toggle switch is a bistable dynamical system, possessing two stable equilibria, each associated to a fully expressed protein, and an unstable equilibrium point, whose stable manifold is the boundary separating the basins of attraction of the two stable coexisting steady states.

Recently, in [6] the problem has been studied of stabilizing a genetic toggle switch (based on the LacI/TetR promoters in *E. coli*), schematically shown in Figure 1, at its unstable equilibrium point. The expression level of the two repressing proteins can be controlled by regulating the concentration of two inducer molecules, aTc and IPTG. The former, aTc, bonds to TetR, increasing the rate of production of LacI, and therefore causing the cell to commit to the stable equilibrium point corresponding to high expression of LacI (high LacI/low TetR). The latter, IPTG bonds instead to LacI, causing the commitment of the cell to the other stable equilibrium point (high TetR/low LacI). From a dynamical systems viewpoint, varying the two input signals causes the

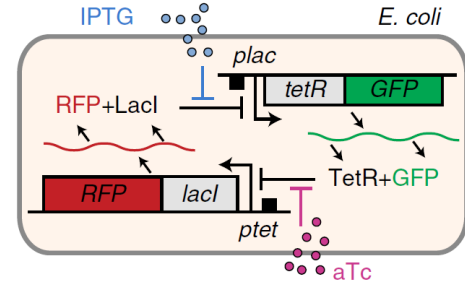


Fig. 1. Genetic toggle switch embedded in *E. coli* considered in from [6] (Figure reused under Creative Commons license).

occurrence of two saddle-node bifurcations changing the phase portrait of the system from bistability to monostability (Figure 2).

In their work Lugagne et al [6] focus on both the problem of controlling a single cell and that of taming the behaviour of the whole population. Their approach is based on considering the toggle switch as a multi-input control system and is aimed at using both inputs to stabilize the switch onto its unstable equilibrium point; a problem they propose as a testbed scenario in synthetic biology similar to that of stabilizing an inverted pendulum in classical control.

When implementing single cell control, the fluorescence level of the reporter proteins in a single cell are measured and compared to their reference values. Two different classes of controllers were used, PI and bang-bang, both designed independently for each control input (aTc and IPTG). Using PI controllers on both input channels, it is possible to make the single cell evolve (oscillate) around the unstable equilibrium point. Although the controlled cell follows (in mean) the desired reference, the rest of the population is observed to drift away from the desired steady state converging instead to some other equilibrium point.

Surprisingly, it is reported in [6] that this undesired effect is absent when the *single* cell is controlled by two independent bang-bang inputs with the rest of the population exhibiting an evolution similar to the target cell in this case. To further explore this effect, the authors then consider an open-loop *periodic stimulation* (two mutually exclusive pulse waves with prescribed width) to control the whole population. Again the whole population is shown to converge to a limit cycle surrounding the unstable equilibrium with a remarkable level of coherence in terms of both mean and standard deviation despite cell-to-cell variability and other phenotypic differences between cells.

<sup>1</sup>Davide Fiore, Agostino Guarino and Mario di Bernardo are with the Department of Electrical Engineering and Information Technology, University of Naples Federico II, Via Claudio 21, 80125 Naples, Italy. [dvd.fiore@gmail.com](mailto:dvd.fiore@gmail.com), [agostinoguarino@gmail.com](mailto:agostinoguarino@gmail.com)

<sup>2</sup>Mario di Bernardo is also with the Department of Engineering Mathematics, University of Bristol, University Walk, BS8 1TR Bristol, U.K. [mario.dibernardo@unina.it](mailto:mario.dibernardo@unina.it)

Using an in-silico model this effect is explained in [6] as due to the fact that using the two control inputs, the phase portrait of the system can be periodically changed from one presenting a unique high-LacI equilibrium point to another with a unique high-TetR equilibrium point. Heuristically, this results in an *average* phase-portrait having a unique attractor in between the former two given that, as conjectured in [6], the cell dynamics and the periodic excitation act on different time-scales. Also, changing the characteristics of the periodic forcing (such as period, width and amplitude of the pulses) shifts the position of the average attractor causing cells to evolve towards a different target solution.

Despite providing some qualitative explanation of the experimental observations, several open questions remain. For instance, what causes the massive reduction in standard deviation between different cells in the population and what the period/duty cycle should be of the control inputs to achieve the desired stabilization. Also, the challenge remains of designing better multi-input *feedback* strategies to control populations of host cells endowed with synthetic toggle switches.

In this paper, we address some of these open problems by providing an analytical investigation of the phenomena reported in [6]. We start by deriving a *quasi-steady state model* of the toggle-switch system proposed therein, using formal averaging techniques for nonlinear systems [7] to derive an autonomous *average vector field*, whose solutions, under some conditions, approximate those of the original time-varying system. To simplify the analysis, we assume that the diffusion of the inducer molecules across the cell membrane is *instantaneous*.

We prove that if the average vector field has a unique attracting equilibrium point, say  $\bar{x}_{av}$ , whose position in the state space depends on the duty cycle  $D$  and on the amplitude of the forcing pulse waves  $u_{aTc}(t)$  and  $u_{IPTG}(t)$ , then every solution of the original time-varying system asymptotically converges to a periodic orbit inside some neighborhood of  $\bar{x}_{av}$ . We compare our model predictions with the experimental observations made in [6] and with the mean-value trajectories of the original model proposed therein. We use the model and its analysis to provide some indications on how the parameters of the toggle switch may be tuned to enhance its response to the class of periodic inputs of interest, and exploit the results to synthesize an external control strategy to regulate the mean-value of the measured fluorescence of the reporting proteins in the cell at some desired value. We wish to emphasize that the analysis provided in this paper can be instrumental for the design of further control strategies for this particularly relevant class of synthetic devices and to investigate the population level effects induced by different types of periodic stimuli to the cells.

## II. MATHEMATICAL MODEL OF THE TOGGLE SWITCH

### A. Transcription-translation model

The deterministic model of the toggle switch that we start from can be given as follows [6]

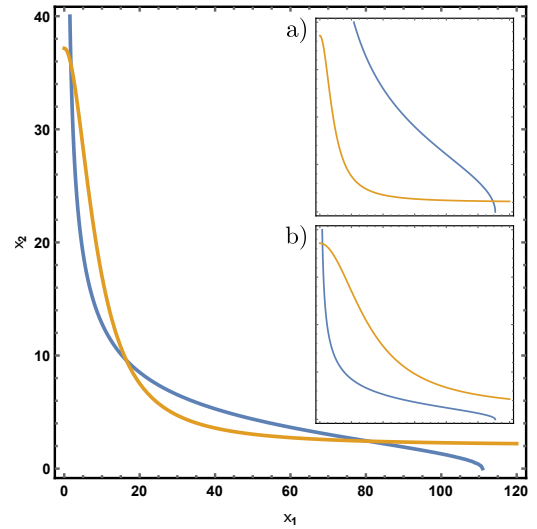


Fig. 2. Nullclines of the toggle switch system (8). Main picture: bistability: two stable and one unstable equilibrium points. Reference values  $aTc = 20$  ng/ml,  $IPTG = 0.25$  mM. Insets: a) monostability: unique high LacI/low TetR equilibrium point.  $aTc = 50$  ng/ml,  $IPTG = 0.25$  mM; b) monostability: unique high TetR/low LacI equilibrium point.  $aTc = 20$  ng/ml,  $IPTG = 0.50$  mM

$$\frac{dmRNA_{LacI}}{dt} = \kappa_L^{m0} + \frac{\kappa_L^m}{1 + \left( \frac{TetR}{\theta_{TetR}} \cdot \frac{1}{1 + (aTc/\theta_{aTc})^{\eta_{aTc}}} \right)^{\eta_{TetR}}} - g_L^m \cdot mRNA_{LacI} \quad (1)$$

$$\frac{dmRNA_{TetR}}{dt} = \kappa_T^{m0} + \frac{\kappa_T^m}{1 + \left( \frac{LacI}{\theta_{LacI}} \cdot \frac{1}{1 + (IPTG/\theta_{IPTG})^{\eta_{IPTG}}} \right)^{\eta_{LacI}}} - g_T^m \cdot mRNA_{TetR} \quad (2)$$

$$\frac{dLacI}{dt} = \kappa_L^p \cdot mRNA_{LacI} - g_L^p \cdot LacI \quad (3)$$

$$\frac{dTetR}{dt} = \kappa_T^p \cdot mRNA_{TetR} - g_T^p \cdot TetR \quad (4)$$

In the above equations the variables denote concentrations of molecules inside the cell, and the parameters  $\kappa_L^{m0}$ ,  $\kappa_L^m$ ,  $\kappa_T^{m0}$ ,  $\kappa_T^m$ ,  $\kappa_L^p$ ,  $\kappa_T^p$ ,  $g_L^p$ ,  $g_T^p$  are leakage transcription, transcription, translation, mRNA degradation, and protein degradation rates, respectively. All their values are provided in [6, Supplementary Table 1] and the same are used in this paper.

The inducer molecules diffuse in and out of the cell across the membrane with non-symmetrical exchange dynamics given by

$$\frac{daTc}{dt} = \begin{cases} k_{aTc}^{in}(u_{aTc} - aTc), & \text{if } u_{aTc} > aTc \\ k_{aTc}^{out}(aTc - u_{aTc}), & \text{if } u_{aTc} \leq aTc \end{cases} \quad (5)$$

$$\frac{dIPTG}{dt} = \begin{cases} k_{IPTG}^{in}(u_{IPTG} - IPTG), & \text{if } u_{IPTG} > IPTG \\ k_{IPTG}^{out}(u_{IPTG} - IPTG), & \text{if } u_{IPTG} \leq IPTG \end{cases} \quad (6)$$

where  $aTc$  and  $IPTG$  denotes the concentrations of the inducer molecules inside the cell,  $u_{aTc}$  and  $u_{IPTG}$  those in the growth medium.

### B. Quasi-steady state model

Assuming that the concentrations of the mRNA molecules reach quasi-steady state more rapidly than their correspond-

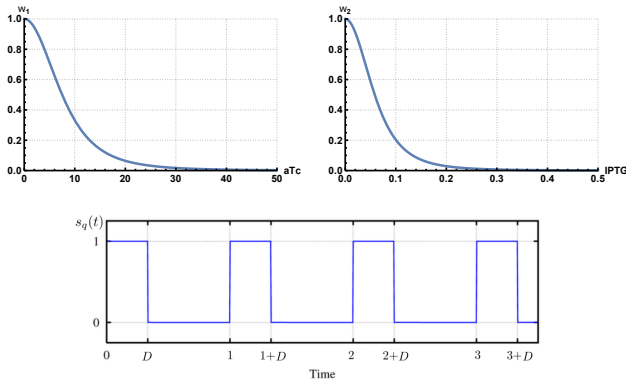


Fig. 3. Top: Static nonlinear functions  $w_1(aTc)$  and  $w_2(IPTG)$  as in (11) and (12). Bottom: Pulse wave  $s_q(t)$ : period 1, duty cycle  $D \in [0, 1]$ .

ing protein, that LacI and TetR proteins degrade at the same rate, that is  $g_L^p = g_T^p = g^p$ , and using the following dimensionless variables (similarly as done in [8], [9])

$$t' = g^p t, \quad x_1 = \frac{LacI}{\theta_{LacI}}, \quad x_2 = \frac{TetR}{\theta_{TetR}}, \quad (7)$$

we obtain the following nondimensional quasi-steady state model of the genetic toggle switch

$$\begin{aligned} \frac{dx_1}{dt'} &= k_1^0 + \frac{k_1}{1 + x_2^2 \cdot w_1(t'/g^p)} - x_1 \\ \frac{dx_2}{dt'} &= k_2^0 + \frac{k_2}{1 + x_1^2 \cdot w_2(t'/g^p)} - x_2 \end{aligned} \quad (8)$$

where

$$k_1^0 = \frac{\kappa_L^{m0} \kappa_L^p}{g_L^m \theta_{LacI} g^p}, \quad k_1 = \frac{\kappa_L^m \kappa_L^p}{g_L^m \theta_{LacI} g^p}, \quad (9)$$

and

$$k_2^0 = \frac{\kappa_T^{m0} \kappa_T^p}{g_T^m \theta_{TetR} g^p}, \quad k_2 = \frac{\kappa_T^m \kappa_T^p}{g_T^m \theta_{TetR} g^p}, \quad (10)$$

are dimensionless parameters, and we have set  $\eta_{LacI} = \eta_{TetR} = 2$ . The steps of the previous derivation are reported in the Appendix.

The nonlinear functions  $w_1(t)$  and  $w_2(t)$  in (8) take into account the static relationship between the repressor protein (TetR or LacI) and their regulator molecule (aTc or IPTG, respectively). They are shown in Figure 3 and are defined as

$$w_1(aTc(t)) = \frac{1}{\left(1 + \left(\frac{aTc(t)}{\theta_{aTc}}\right)^{\eta_{aTc}}\right)^{\eta_{TetR}}} \quad (11)$$

$$w_2(IPTG(t)) = \frac{1}{\left(1 + \left(\frac{IPTG(t)}{\theta_{IPTG}}\right)^{\eta_{IPTG}}\right)^{\eta_{LacI}}} \quad (12)$$

System (8) with the static relations (11)-(12) and diffusion dynamics across the cell membrane (5)-(6) can be represented in block form as in Figure 4. The cell membrane acts as a linear (non-symmetrical) first order low-pass filter for the signals  $u_{aTc}(t)$  and  $u_{IPTG}(t)$  with a cut-off frequency that depends on the diffusion exchange rates  $k_{aTc}^{in/out}$  and  $k_{IPTG}^{in/out}$ . Hence,  $aTc(t)$  and  $IPTG(t)$  are filtered version of their

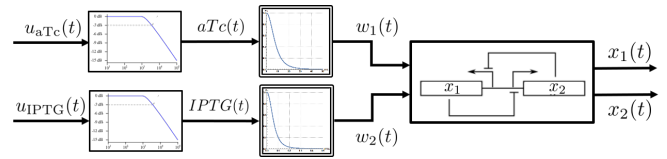


Fig. 4. Block diagram of system (8) with diffusion dynamics across the cell membrane (5)-(6).

respective input signals whose attenuation depends both on the cut-off frequency and on their spectral density.

In our analysis we make the following simplifying assumption.

*Assumption 1:* The diffusion dynamics of the inducer molecules, aTc and IPTG, across the cell membrane is instantaneous, that is

$$aTc(t) = u_{aTc}(t), \quad (13)$$

$$IPTG(t) = u_{IPTG}(t), \quad (14)$$

for every  $t \geq t_0$ .

Later in Section IV, we will compare our results derived from system (8) under the above Assumption 1 with the solutions of the complete toggle switch model (1)-(4) with more realistic diffusion dynamics given by (5)-(6).

### III. AVERAGING ANALYSIS OF THE TOGGLE SWITCH UNDER PULSE WAVE INPUT SIGNALS

#### A. Forcing signals

The concentrations of the inducers in the growth medium are considered to vary in time as two mutually exclusive pulse waves of period  $T$ , duty cycle  $D \in [0, 1]$  and amplitude  $\bar{u}_{aTc}$  and  $\bar{u}_{IPTG}$ , respectively, that is

$$u_{aTc}(t) = \bar{u}_{aTc} \cdot (1 - s_q(t/T)) \quad (15)$$

$$u_{IPTG}(t) = \bar{u}_{IPTG} \cdot s_q(t/T) \quad (16)$$

where  $s_q(t)$  is the pulse wave taking values 0 and 1, with period 1 and duty cycle  $D$ , reported in Figure 3. In the experiments described in [6], the amplitude  $\bar{u}_{aTc}$  and  $\bar{u}_{IPTG}$  were allowed to take values between 0 and 100 ng/ml, and 0 and 1 mM, respectively.

Note that  $D = 0$  corresponds to “high aTc/no IPTG” in the growth medium which in turns results in full steady-state expression of LacI (high  $x_1$ ). Likewise,  $D = 1$  corresponds to “no aTc/high IPTG” yielding full expression of TetR (high  $x_2$ ). Therefore, the duty cycle can be used to control the ratio between the activation time of the two monostable systems associated to the presence or absence of the two inducer molecules whose nullclines are shown in the insets in Figure 2.

Under Assumption 1 it follows that

$$\begin{aligned} w_1(t) &= w_1(aTc(t)) \\ &= w_1(\bar{u}_{aTc} \cdot (1 - s_q(t/T))) \\ &= \bar{w}_1 + (1 - \bar{w}_1) \cdot s_q(t/T), \end{aligned} \quad (17)$$

where  $\bar{w}_1 = w_1(\bar{u}_{aTc})$ , and

$$\begin{aligned} w_2(t) &= w_2(IPTG(t)) \\ &= w_2(\bar{u}_{IPTG} \cdot s_q(t/T)) \\ &= \bar{w}_2 + (1 - \bar{w}_2) \cdot (1 - s_q(t/T)), \end{aligned} \quad (18)$$

where  $\bar{w}_2 = w_2(\bar{u}_{IPTG})$ . Therefore,  $w_i(t)$  is a pulse wave taking values between 1 and  $\bar{w}_i$ .

### B. Average vector field

By rescaling time setting  $\tau = \frac{t'}{Tg^p}$ , system (8) can be recast as

$$\begin{aligned} \frac{dx_1}{d\tau} &= \varepsilon \left[ k_1^0 + \frac{k_1}{1 + x_2^2 \cdot w_1(\tau T)} - x_1 \right] \\ \frac{dx_2}{d\tau} &= \varepsilon \left[ k_2^0 + \frac{k_2}{1 + x_1^2 \cdot w_2(\tau T)} - x_2 \right] \end{aligned} \quad (19)$$

with  $\varepsilon = Tg^p$ . The vector field in (19) is time-varying in  $\tau$  with period 1, and it is now in a form amenable for periodic averaging analysis (see Appendix).

In particular, the average vector field, say  $f_{av}(x)$ , can be obtained by integrating the vector field in (19) over a period, yielding

$$\begin{aligned} f_{av,1}(x) &= \frac{1}{1} \int_0^1 \left( k_1^0 + \frac{k_1}{1 + x_2^2 \cdot w_1(\tau T)} - x_1 \right) d\tau \\ &= k_1^0 + k_1 \left( \int_0^D \frac{1}{1 + x_2^2 \cdot 1} d\tau + \int_D^1 \frac{1}{1 + x_2^2 \cdot \bar{w}_1} d\tau \right) - x_1 \\ &= k_1^0 + k_1 \left( \frac{D}{1 + x_2^2} + \frac{1 - D}{1 + x_2^2 \cdot \bar{w}_1} \right) - x_1, \end{aligned}$$

where we used (17), and similarly for  $f_{av,2}(x)$ ,

$$\begin{aligned} f_{av,2}(x) &= \frac{1}{1} \int_0^1 \left( k_2^0 + \frac{k_2}{1 + x_1^2 \cdot w_2(\tau T)} - x_2 \right) d\tau \\ &= k_2^0 + k_2 \left( \int_0^D \frac{1}{1 + x_1^2 \cdot \bar{w}_2} d\tau + \int_D^1 \frac{1}{1 + x_1^2 \cdot 1} d\tau \right) - x_2 \\ &= k_2^0 + k_2 \left( \frac{D}{1 + x_1^2 \cdot \bar{w}_2} + \frac{1 - D}{1 + x_1^2} \right) - x_2, \end{aligned}$$

where we used (18).

Hence, the resulting *average system* is

$$\begin{aligned} \frac{dx_1}{d\tau} &= \varepsilon \left[ k_1^0 + k_1 \left( \frac{D}{1 + x_2^2} + \frac{1 - D}{1 + x_2^2 \cdot \bar{w}_1} \right) - x_1 \right] \\ \frac{dx_2}{d\tau} &= \varepsilon \left[ k_2^0 + k_2 \left( \frac{D}{1 + x_1^2 \cdot \bar{w}_2} + \frac{1 - D}{1 + x_1^2} \right) - x_2 \right] \end{aligned} \quad (20)$$

Let  $x(\tau, \varepsilon)$  and  $x_{av}(\varepsilon\tau)$  denote the solutions of (19) and (20), respectively. Assume  $\bar{x}_{av}$  is an exponentially stable equilibrium point of the average system (20). Let  $\Omega$  be a compact subset of its basin of attraction, and assume  $x_{av}(0) \in \Omega$ , and  $x(0, \varepsilon) - x_{av}(0) = O(\varepsilon)$ . Then, from [7, Theorem 10.4], there exists a positive parameter  $\varepsilon^* = T^*g^p$  such that for all  $0 < \varepsilon < \varepsilon^*$

$$x(\tau, \varepsilon) - x_{av}(\varepsilon\tau) = O(\varepsilon) \quad (21)$$

for all  $\tau > 0$ . That is, solutions  $x(\tau, \varepsilon)$  to system (19) can be approximated by solutions  $x_{av}(\varepsilon\tau)$  with an error that is

proportional to  $\varepsilon$ . As a consequence, if  $\bar{x}_{av}$  is the unique equilibrium point of system (20), then for all  $0 < \varepsilon < \varepsilon^*$  system (19) has a unique stable periodic solution  $\bar{x}(\tau, \varepsilon)$  in a  $O(\varepsilon)$ -neighborhood of  $\bar{x}_{av}$ .

The number and position in the state space of the equilibrium points  $\bar{x}_{av}$  of the average system (20) depend on the specific choice of the amplitude  $\bar{u}_{aTc}$  and  $\bar{u}_{IPTG}$  of the pulse waves, and also on the value of the duty cycle  $D$ . For example, for the reference values  $\bar{u}_{aTc} = 50 \text{ ng/ml}$  and  $\bar{u}_{IPTG} = 0.5 \text{ mM}$ , system (20) is monostable and the position of the equilibrium point  $\bar{x}_{av}$  varies with  $D$  as reported in Figure 5(a) (blue dots). Hence, given certain values of  $\bar{u}_{aTc}$  and  $\bar{u}_{IPTG}$ , it is possible to move the position of  $\bar{x}_{av}$  on the corresponding curve by varying  $D$  (Figures 5(b) and 5(c)).

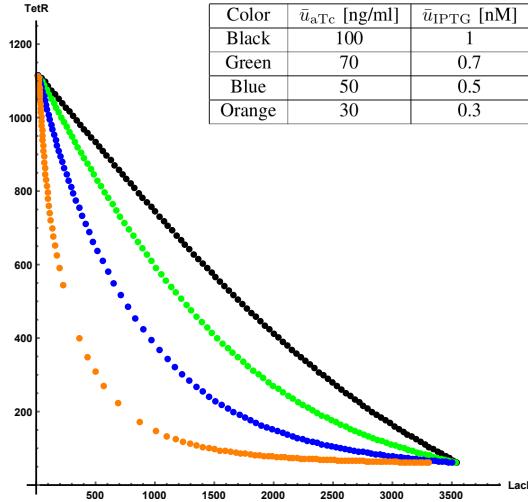
The phase portrait of the average system (20) together with representative solutions of the time-varying system (19) for  $D$  equal to 0.2 and 0.8 are depicted in Figures 6(a) and 6(b), respectively. The parameter  $\varepsilon$  has been set to 0.1 which corresponds to a forcing period  $T = \varepsilon/g^p \approx 6 \text{ min}$ , and the system has been simulated for  $t_f = \tau_f T \approx 50 \cdot 6 = 300 \text{ min}$ . Larger values of  $\varepsilon$  correspond to larger values of the forcing period  $T$ . In turn, from (21), this also implies that the solution  $x(\tau, \varepsilon)$  of (19) will asymptotically converge to a periodic solution  $\bar{x}(\tau, \varepsilon)$  contained in a larger set (Figure 7(b)), and hence to a worse approximation.

## IV. DIFFUSION EFFECTS

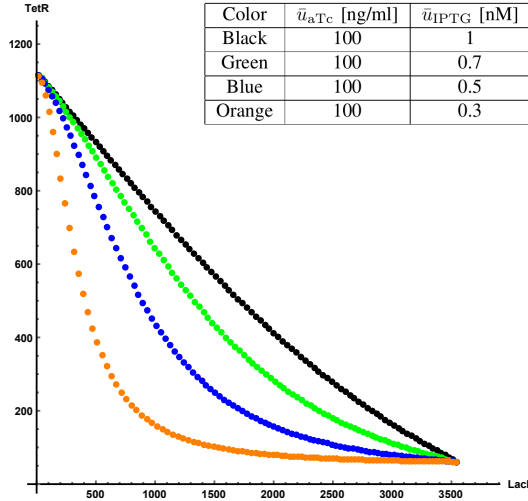
The analysis in the previous section was conducted under Assumption 1. As already mentioned before, the cell membrane acts as a low-pass filter, hence, when Assumption 1 is dropped,  $aTc(t)$  and  $IPTG(t)$  will not anymore be ideal pulse waves but their filtered versions. Therefore, in order that the average system (20) will still be a good approximation of the actual cell response, the cut-off frequency of the two low-pass filters should be sufficiently higher than the fundamental frequency  $1/T$  of the input pulse waves. However, due to the inevitable attenuation of high-frequency harmonics, there will always be a mismatch between the actual mean cell response and the value predicted by (20).

In Figure 8 we report the comparison, for two different combinations of the amplitudes of the pulse waves and varying the duty cycle  $D$ , between the mean steady-state response of the complete four-dimensional system (1)-(4) with diffusion dynamics (5)-(6), and the corresponding equilibrium point  $\bar{x}_{av}(D)$  predicted by the autonomous two-dimensional average system (20). Although there is not a perfect correspondence between the two, the observed behaviour is well captured by the average system. Note that in regulation problems, this mismatch can be compensated by designing an adequate feedback action.

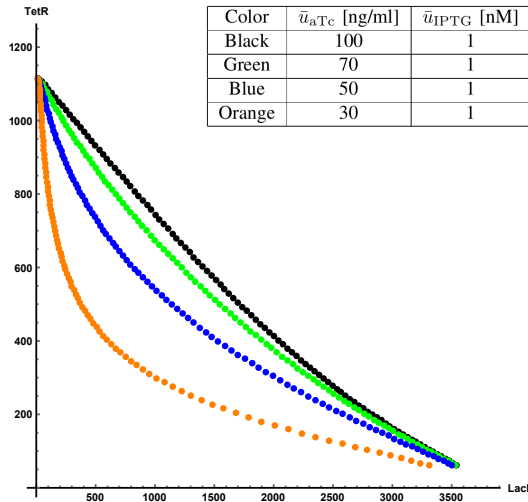
On the other hand, when the fundamental frequency  $1/T$  of the input pulse waves is higher of the cut-off frequency of one of the filters, the input signal will be highly attenuated, resulting in a simple regulation of the toggle switch to either one of the stable equilibrium points (a phenomenon that was reported in the experiments described in [6, Supplementary



(a) Equilibrium points for different values of  $\bar{u}_{aTc}$  and  $\bar{u}_{IPTG}$ .

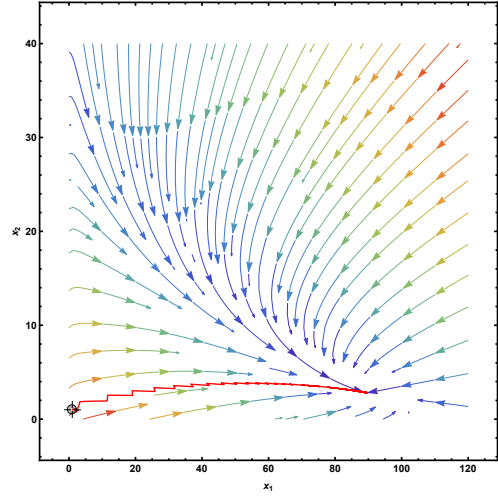


(b) Equilibrium points for  $\bar{u}_{aTc} = 100$  ng/ml and different values of  $\bar{u}_{IPTG}$ .

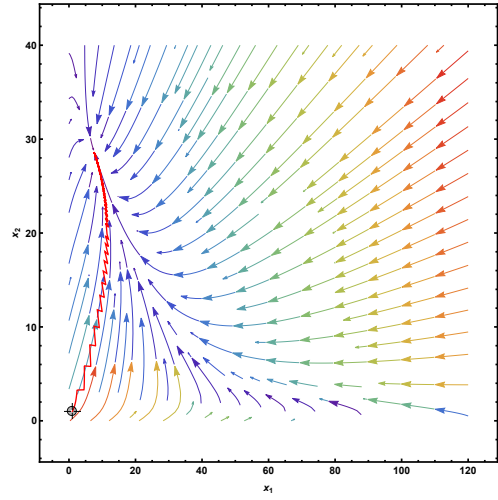


(c) Equilibrium points for  $\bar{u}_{IPTG} = 1$  mM and different values of  $\bar{u}_{aTc}$ .

Fig. 5. Equilibrium points  $\bar{x}_{av}$  of (20) as a function of duty cycle  $D$  rescaled in arbitrary fluorescence units using (7). Each dot represents the location of the unique stable equilibrium point of system (20) evaluated for  $D$  taking values in the interval  $[0, 1]$  with increments of 0.01.



(a)  $D = 0.2$ ,  $T \approx 6$  min ( $\varepsilon = 0.1$ ).



(b)  $D = 0.8$ ,  $T \approx 6$  min ( $\varepsilon = 0.1$ ).

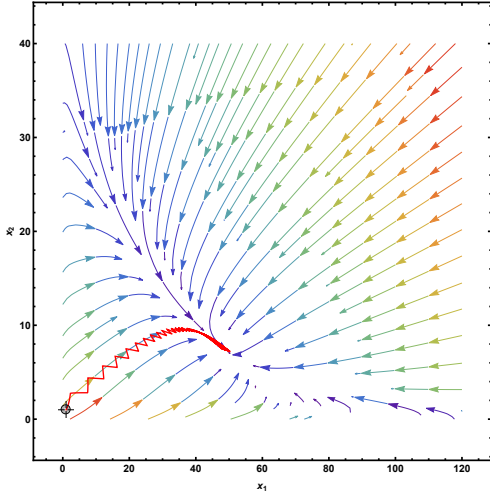
Fig. 6. Background: phase portrait of the average system (20). Red line: the solution of the time-varying system (19) with  $\bar{u}_{aTc} = 50$  ng/ml and  $\bar{u}_{IPTG} = 0.5$  mM from initial condition  $[1, 1]^T$ .

Figure 8)]. A similar phenomenon can also occur when the duty cycle is close to 0 or 1. Indeed, close to these values, the amplitude of the harmonics of a pulse wave is  $|a_n| = \left| \frac{2\bar{u}}{n\pi} \sin(n\pi D) \right| \approx 2\bar{u}D$ , therefore low-frequency harmonics will have amplitudes similar to those of high-frequency ones, and the pulse wave will be highly attenuated.

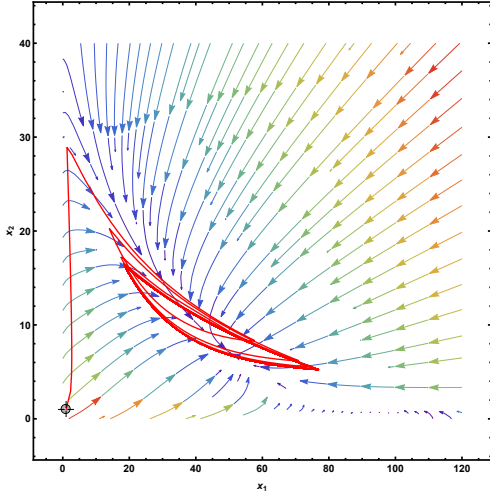
## V. PERSPECTIVES FOR CONTROL

We wish to emphasize that the analytical results derived here can also be used for the synthesis of external controllers to regulate the mean-value of the output response of the genetic toggle switch. Specifically, we propose the control schematic shown in Figure 9 which is currently under development and will be presented elsewhere. Indeed, as done in Figure 5, it is possible to numerically compute  $\bar{x}_{av}$  as a function of  $\bar{u}_{aTc}$ ,  $\bar{u}_{IPTG}$  and  $D$ , and get interpolating curves  $\gamma_{\bar{u}_{aTc}, \bar{u}_{IPTG}}(D)$ . From these one can then obtain, for given values of the amplitude  $\bar{u}_{aTc}$  and  $\bar{u}_{IPTG}$ , the duty cycle





(a)  $D = 0.5$ ,  $T \approx 6$  min ( $\varepsilon = 0.1$ ).



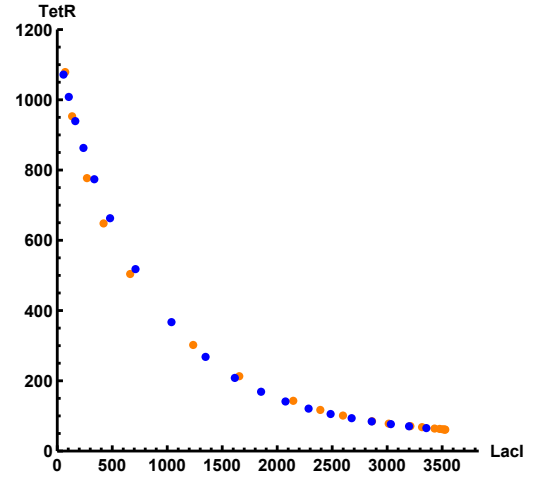
(b)  $D = 0.5$ ,  $T \approx 180$  min ( $\varepsilon = 3$ ).

Fig. 7. Background: phase portrait of the average system (20). Red line: the solution of the time-varying system (19) with  $\bar{u}_{aTc} = 50$  ng/ml and  $\bar{u}_{IPTG} = 0.5$  mM from initial condition  $[1, 1]^T$ .

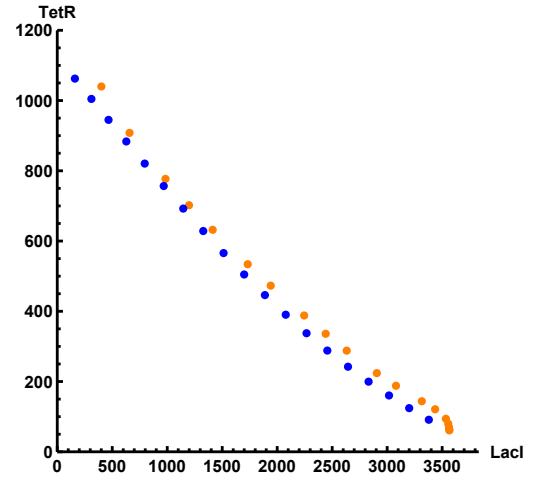
$D_{ref}$  corresponding to the desired average set-point  $\bar{x}_{av}^{ref}$ , that is  $D_{ref} = \gamma_{\bar{u}_{aTc}, \bar{u}_{IPTG}}^{-1}(\bar{x}_{av}^{ref})$ . The mismatch  $e$  between the measured mean-value of the plant outputs and  $\bar{x}_{av}^{ref}$  is then projected by  $\pi$  onto the curve  $\gamma_{\bar{u}_{aTc}, \bar{u}_{IPTG}}$  and compensated by a PI controller. The control scheme should also take into account the effects of the sampling time and of the slow transients.

## VI. CONCLUSIONS

We derived and analysed a model to capture the response of the genetic toggle switch to mutually exclusive pulse waves as observed experimentally in [6]. The analysis was based on the assumption that the diffusion of inducer molecules across the cell membrane is instantaneous. From this, using the periodic averaging method for nonlinear systems, we derived an autonomous vector field that describes the dynamics of the mean-value of the periodic solutions of the original system. After discussing the predictions of



(a) Amplitude of pulse waves set to  $\bar{u}_{aTc} = 50$  ng/ml and  $\bar{u}_{IPTG} = 0.5$  mM.



(b) Amplitude of pulse waves set to  $\bar{u}_{aTc} = 100$  ng/ml and  $\bar{u}_{IPTG} = 1$  mM.

Fig. 8. Orange dots: Mean-value, evaluated at regime, of the response of system (1)-(4) (with membrane dynamics (5)-(6)) to pulse waves with  $T = 240$  min and varying  $D$  from 0.05 to 0.95 with increments of 0.05. Blue dots: corresponding equilibrium point  $\bar{x}_{av}(D)$  of system (20).

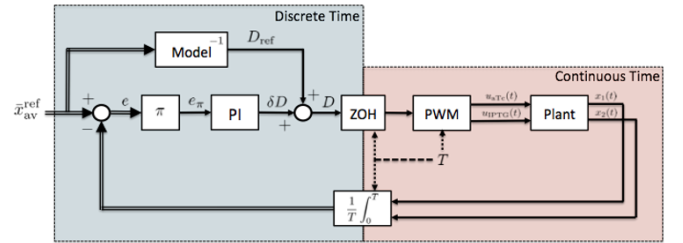


Fig. 9. External controller for the regulation of the mean-response of a genetic toggle switch.

the model under the assumption of instantaneous diffusion, we relaxed this assumption so that the input signals become filtered versions of themselves worsening the in-silico prediction.

However, even if it is not possible to eliminate the

attenuation due to the cell membrane, our analysis shows that to mitigate its effects the frequency  $1/T$  of the input pulse waves should be chosen sufficiently lower than the cut-off frequency of the low-pass membrane filter, and extreme values of the duty cycle  $D$  should be avoided. At the same time, we find that to avoid large oscillations around  $\bar{x}_{av}$ , the parameter  $\varepsilon = Tg^p$ , that is the ratio between the time-scales of the forcing inputs and system dynamics, should be taken as small as possible, e.g., for fixed  $T$ , by cooling down the temperature of the growth medium and thus reducing the cell growth rate and therefore  $g^p$ .

Future work will be aimed at quantifying the effects of the attenuation of the input signals due to the cell membrane to improve the predictions of our model, and at implementing and validating (in-silico and in-vivo) external controllers, also capable of modulate the ON/OFF values of the pulse waves. Furthermore, we also plan to investigate the effect that different classes of periodic forcing could have on the variance of the response of a population of cells with extrinsic noise.

## APPENDIX

### Periodic averaging

We recall here that, from [7, Theorem 10.4], the periodic averaging method says that the solutions of the system

$$\dot{x} = \varepsilon f(t, x, \varepsilon) \quad (22)$$

where  $f(\cdot)$  is sufficiently smooth with respect to  $(x, \varepsilon)$ , and  $T$ -periodic and measurable in  $t$ , can be approximated by an autonomous average system

$$\dot{x} = \varepsilon f_{av}(x) \quad (23)$$

where  $f_{av}(x) = \frac{1}{T} \int_0^T f(s, x, 0) ds$ . More precisely, if system (23) has an exponentially stable equilibrium point  $\bar{x}_{av}$ , then there exist positive constants  $\varepsilon^*$  and  $k$  such that, for all  $0 < \varepsilon < \varepsilon^*$ , system (22) has a unique, exponentially stable,  $T$ -periodic solution  $\bar{x}(t, \varepsilon)$  in a  $O(\varepsilon)$ -neighborhood of  $\bar{x}_{av}$ , that is  $\|\bar{x}(t, \varepsilon) - \bar{x}_{av}\| \leq k\varepsilon$ . Moreover, if the initial conditions are such that  $x(0, \varepsilon) - x_{av}(0) = O(\varepsilon)$ , then  $x(t, \varepsilon) - x_{av}(\varepsilon t) = O(\varepsilon)$ , for all  $t \geq 0$ .

### Nondimensionalization of system (1)-(4)

Equations (1) and (2) can be rewritten as

$$\begin{aligned} \frac{dmRNA_{LacI}}{dt} &= \kappa_L^{m0} + \frac{\kappa_L^m}{1 + \left(\frac{TetR}{\theta_{TetR}}\right)^{\eta_{TetR}} \cdot w_1(t)} - g_L^m \cdot mRNA_{LacI} \\ \frac{dmRNA_{TetR}}{dt} &= \kappa_T^{m0} + \frac{\kappa_T^m}{1 + \left(\frac{LacI}{\theta_{LacI}}\right)^{\eta_{LacI}} \cdot w_2(t)} - g_T^m \cdot mRNA_{TetR} \end{aligned}$$

where  $w_1(t)$  and  $w_2(t)$  are defined in (11)-(12).

Now, taking into account that mRNA molecules are degraded faster than other molecules, we can obtain a quasi-steady state approximation by setting  $\frac{dmRNA_{LacI}}{dt} = 0$  and  $\frac{dmRNA_{TetR}}{dt} = 0$ , yielding

$$\begin{aligned} mRNA_{LacI} &= \frac{\kappa_L^{m0}}{g_L^m} + \frac{\kappa_L^m}{g_L^m} \frac{1}{1 + \left(\frac{TetR}{\theta_{TetR}}\right)^{\eta_{TetR}} \cdot w_1(t)} \\ mRNA_{TetR} &= \frac{\kappa_T^{m0}}{g_T^m} + \frac{\kappa_T^m}{g_T^m} \frac{1}{1 + \left(\frac{LacI}{\theta_{LacI}}\right)^{\eta_{LacI}} \cdot w_2(t)} \end{aligned}$$

Assuming that LacI and TetR proteins degrade at the same rate, that is  $g_L^p = g_T^p = g^p$ , that  $\eta_{LacI} = \eta_{TetR} = 2$ , and using the dimensionless state variables and time  $t' = g^p t$ ,  $x_1 = \frac{LacI}{\theta_{LacI}}$ ,  $x_2 = \frac{TetR}{\theta_{TetR}}$ , we obtain from (3)

$$\begin{aligned} \frac{dx_1}{dt'} &= \frac{\kappa_L^p}{\theta_{LacI} g^p} mRNA_{LacI} - x_1 \\ &= \frac{\kappa_L^p}{\theta_{LacI} g^p} \left[ \frac{\kappa_L^{m0}}{g_L^m} + \frac{\kappa_L^m}{g_L^m} \frac{1}{1 + x_2^2 \cdot w_1(t'/g^p)} \right] - x_1 \\ &= k_1^0 + \frac{k_1}{1 + x_2^2 \cdot w_1(t'/g^p)} - x_1 \end{aligned}$$

with  $k_1^0$  and  $k_1$  as in (9), and from (4)

$$\begin{aligned} \frac{dx_2}{dt'} &= \frac{\kappa_T^p}{\theta_{TetR} g^p} mRNA_{TetR} - x_2 \\ &= \frac{\kappa_T^p}{\theta_{TetR} g^p} \left[ \frac{\kappa_T^{m0}}{g_T^m} + \frac{\kappa_T^m}{g_T^m} \frac{1}{1 + x_1^2 \cdot w_2(t'/g^p)} \right] - x_2 \\ &= k_2^0 + \frac{k_2}{1 + x_1^2 \cdot w_2(t'/g^p)} - x_2 \end{aligned}$$

with  $k_2^0$ ,  $k_2$  as in (10).

## ACKNOWLEDGMENT

This manuscript has resulted from the COSY-BIO (Control Engineering of Biological Systems for Reliable Synthetic Biology Applications) project, that has received funding from the European Union's Horizon 2020 research and innovation programme under grant agreement No 766840.

## REFERENCES

- [1] U. Alon, *An introduction to systems biology: design principles of biological circuits*. CRC press, 2006.
- [2] L. Chen, R. Wang, C. Li, and K. Aihara, *Modeling biomolecular networks in cells*. Springer-Verlag London, 2010.
- [3] T. S. Gardner, C. R. Cantor, and J. J. Collins, "Construction of a genetic toggle switch in *escherichia coli*," *Nature*, vol. 403, no. 6767, pp. 339–342, 2000.
- [4] T. Tian and K. Burrage, "Stochastic models for regulatory networks of the genetic toggle switch," *Proceedings of the National Academy of Sciences*, vol. 103, no. 22, pp. 8372–8377, 2006.
- [5] M. Wu, R.-Q. Su, X. Li, T. Ellis, Y.-C. Lai, and X. Wang, "Engineering of regulated stochastic cell fate determination," *Proceedings of the National Academy of Sciences*, vol. 110, no. 26, pp. 10610–10615, 2013.
- [6] J.-B. Lugagne, S. S. Carrillo, M. Kirch, A. Köhler, G. Batt, and P. Hersen, "Balancing a genetic toggle switch by real-time feedback control and periodic forcing," *Nature Communications*, vol. 8, no. 1, p. 1671, 2017.
- [7] H. K. Khalil, *Nonlinear systems*, 2002.
- [8] A. Kuznetsov, M. Kærn, and N. Kopell, "Synchrony in a population of hysteresis-based genetic oscillators," *SIAM Journal on Applied Mathematics*, vol. 65, no. 2, pp. 392–425, 2004.
- [9] E. V. Nikolaev and E. D. Sontag, "Quorum-sensing synchronization of synthetic toggle switches: A design based on monotone dynamical systems theory," *PLoS Computational Biology*, vol. 12, no. 4, p. e1004881, 2016.